GEOPHYSICS

Small effect of partial melt on electrical anomalies in the asthenosphere

Hanyong Liu[1], Xiaozhi Yang[1,2]*, Shun-ichiro Karato[3]

High conductivity anomalies in the shallow mantle are frequently attributed to minor partial melt (basalt or carbonatite) in the olivine-dominated peridotites. Conductivity of a melt-mineral mixture depends on the configuration of melt that could be affected by grain size of the constitutive mineral(s), but this has rarely been explored. Here, we provide experimental evidence using a conductive carbonatite analog and olivine that the bulk conductivity decreases systematically with increasing olivine grain size. The required amount of melt for producing the geophysically resolved high conductivities in the asthenosphere is much greater than previously assumed. We suggest that the effect of partial melt on many conductive regions in the asthenosphere is small. Instead, the electrical anomalies (especially those away from mid-ocean ridges) originate more likely from subsolidus solid assemblages in the upper mantle. This reconciles well the geochemical and petrological constraints of the shallow mantle with its geophysically determined electrical properties.

INTRODUCTION

The presence of a mechanically weak asthenosphere underlying the rigid lithospheric lid is a prerequisite for plate tectonics. Studies of deep magnetotelluric surveys reveal high conductivity areas of ~0.01 to >0.1 S/m at a depth of ~40 to 110 km in the shallow mantle, which are broadly independent of the lithospheric age and are often assumed to be consistent with the depth of the seismologically defined asthenosphere particularly beneath oceans (*1*–*3*). The conductive zones are frequently explained by the presence of a small amount of partial melt, such as ~0.5 to 1 vol % of basalt or 0.05 to 0.5 vol % of carbonatite or carbonated basalt (*3*–*8*). Melt of these fractions, and even less, in the asthenosphere is likely to be compatible with petrological and physical constraints (*9*–*11*). If the volume amount is greater, then melt is difficult to maintain over a broad region (in the shallow mantle) and should be driven out because of melt extraction and efficient compaction of the system (*9*, *12*).

The upper mantle is dominated by peridotite, a rock consisting mainly of olivine and pyroxenes. Olivine is the most abundant mineral, with 60 to 80 vol % in lherzolite to more than 90 vol % in dunite, and greatly determines the electrical structure of the upper mantle because other minerals in peridotites are usually texturally isolated and do not form interconnected networks (thus, contributing little, if any, to bulk conductivity). Accordingly, the estimation of the required melt amount for causing the observed high conductivity has been commonly done by (i) measuring the conductivity of melt (basalt/carbonatite) and olivine separately and then modeling the bulk conductivity of a melt-olivine system with different melt fractions (*1*, *4*, *6*) or (ii) determining directly the conductivity of a melt-olivine system with fine-grained (e.g., <10 μm) olivine (*5*, *7*). However, in either case, the effect of olivine grain size, which may affect the edges and corners of grain boundaries in the system and the topology and connectivity of melt along the grain boundaries, on the bulk conductivity has not been explored. Here, we have experimentally examined the influence of mineral grain size on melt-olivine conductivity. We show that the conductivity decreases with increasing olivine grain size and that, for typical grain sizes of minerals in the upper mantle, the amount of melt needed for high conductivities is greater than previous estimates.

Conductivity measurements of a mantle melt or melt-olivine system, often conducted beyond ~1200°C (for melt formation), are subjected to new mineral crystallization, olivine regrowth, melt-olivine reactions, and/or olivine dissolution in melts (*5*–*7*). Those processes make the system complex, involving not only the transfer of charge carriers but also other thermal processes, and the analyses of conductivity and activation enthalpy are influenced. To overcome these issues, we carried out the experiments at low temperature using a highly mobile and conductive LiNaK carbonatite analog and dry olivine of contrasting grain sizes. The carbonatite was made from Li_2CO_3, Na_2CO_3, and K_2CO_3 powders, which were predried at 200°C for dehydration and mixed in a weight proportion of 32.1:33.4:34.5% (*13*). At room pressure, the carbonatite melts and decarbonates at ~401° and 707°C, respectively (*13*). The dry olivine was carefully prepared by crystal grinding, sieving, annealing, and heating and was then mixed with the carbonatite by accurately weighing the two components (with precision of 0.01 mg). The mixtures were cold-pressed into cylinders of 3.0-mm diameter and ~1.7-mm length. The conductivity runs were done at 1 GPa and 200° to 700°C in a piston cylinder press. The impedance spectra of the samples were collected using a Solartron 1260 analyzer by sweeping at 10^6 to 1 Hz and with different heating-cooling cycles in each run. The resistance (R) before and after the melting of the LiNaK carbonatite was obtained by fitting the spectral arc at high frequency and from the spectral intercept with axis (fig. S2), respectively, as commonly applied to solids (*14*–*19*) and melts/melt-olivine mixtures (*4*–*7*). The conductivity (σ) was calculated by $\sigma = L/(SR)$, where L is the length and S is the effective cross-sectional area of the recovered samples. The uncertainty of conductivity is mostly <10%.

[1]State Key Laboratory for Mineral Deposits Research, School of Earth Sciences and Engineering, Nanjing University, Nanjing 210023, China. [2]Frontiers Science Center for Critical Earth Material Cycling, Nanjing University, Nanjing 210023, China. [3]Department of Earth and Planetary Sciences, Yale University, New Haven, CT 06520, USA.
*Corresponding author. Email: xzyang@nju.edu.cn

RESULTS AND DISCUSSION

In melt-bearing samples, the dihedral angles in triple junctions are 25° to 30° (figs. S3 and S4), agreeing well with those reported for carbonatite-olivine (*20*). During the conductivity runs, the grain size distribution of olivine remains almost unchanged (Table 1 and fig. S5), and the composition of olivine displays nearly no change (table S1), indicating negligible reactions between the carbonatite and olivine. The sample conductivity is described by

$$\sigma = A \cdot \exp\left(-\frac{\Delta H}{\mathrm{R} \cdot T}\right) \quad (1)$$

where A is a pre-exponential factor, ΔH is the activation enthalpy, R is the gas constant, and T is the temperature. The conductivities in the first heating cycle show a jump by approximately two to three orders of magnitude at 400° to 450°C (fig. S6), indicating the carbonatite melting and the connection of melt networks. The data in this cycle are subjected to nonequilibrium melt distribution and are excluded from analysis. The conductivity data above 450°C are presented in Fig. 1. For each run, the data are reproducible between different cycles. This, along with the almost same resistance over a long duration under otherwise identical conditions in a given run (fig. S7), suggests the absence of system hysteresis and the attainment of run equilibrium. Similar arguments have been made for conductivity work on other melt-containing systems (*5*, *7*). Textural equilibrium of the mixed melt-olivine over the studied conditions (Materials and Methods) is not unexpected, because the high mobility (*20*, *21*) and high diffusivity of elements (*22*) in carbonatite melts, particularly those rich in Li, Na, and K, make it easy to change olivine morphology especially at small grain sizes (*23*–*25*). Parameters by fitting the data to Eq. 1 are given in Table 1. At the same olivine grain size (~2.3 μm), the conductivity increases with increasing melt fraction from 0 to ~10 vol %, and the general trend resembles that observed for basalt-olivine and Ca- and Mg-rich carbonatite-olivine at >1200°C (*5*, *7*). Given the same melt fraction (~2 vol %), the conductivity decreases with increasing olivine grain size from ~0.5 to 20 μm. At a given temperature, the conductivity of the melt-olivine mixtures is lower than that of the LiNaK carbonatite melt (*4*) but higher than that of dry olivine. The activation enthalpy of the melt-olivine samples, 32 to 37 kJ/mol, resembles that of the LiNaK carbonatite (*4*), ~33 kJ/mol, but is much smaller than that of dry olivine, 136 to 138 kJ/mol (Table 1) (*15*, *16*, *19*).

The conductivity of a polycrystalline olivine with grain sizes of ~2.3 and 20 μm and a single-crystal olivine is essentially the same (fig. S8), indicating a negligible effect of grain size as expected for lattice conduction in dry olivine (*26*) and also shown for clinopyroxene (*18*). The similar activation enthalpy between the melt-olivine samples, regardless of olivine grain size and melt fraction, and between melt-olivine samples and the LiNaK carbonatite melt (*4*) implies the same mechanism of electrical conduction. For each of the melt-containing samples, the conduction includes the contribution from both grain boundary melt and lattice olivine. The very low conductivity of olivine at similar conditions (Fig. 1) suggests its negligible role in contributing to the bulk conductivity of the melt-olivine samples. Hence, the conductivity of the mixed melt-olivine system is dominated by conductive melt in grain boundaries. This is supported by the dependence of the conductivity on olivine grain size and the enhanced conductivity of the melt-olivine samples relative to olivine. The conduction is controlled by the transfer of Li^+, Na^+, and K^+ (*4*) in the melt networks. The higher conductivity of the melt-olivine mixture at a smaller grain size of olivine under otherwise identical conditions (e.g., 2 vol % of melt) (Fig. 1) implies a systematic grain size effect. This is unexpected for the "ideal" self-similar melt geometry (with respect to grain size) in melt-mineral mixtures, where the conductivity is independent of mineral grain size (Materials and Methods). Given textural

Table 1. Summary of samples and fit parameters. Grain size is the mean value of olivine before (initial) and after (final) the conductivity run. *L*/*S* is the geometric factor of recovered samples (see text). Equation 1 is used to obtain the fit parameters (fit parameters by Eq. 2 are given in table S2).

	Initial grain size of olivine (μm)	Final grain size of olivine (μm)	Melt fraction (vol %)	*L*/*S* (m^{-1})	Log[*A* (S/m)]	Δ*H* (kJ/mol)
Linear fitting for runs on dry olivine (600° to 1350°C)						
B333	2.3 ± 0.3	2.3 ± 0.2		266	3.47 ± 0.20	138 ± 5
A255	20 ± 3	21 ± 2		327	3.32 ± 0.29	136 ± 6
Single crystal*				288/334	3.33 ± 0.07	136 ± 2
Global fitting for runs on dry olivine						
					3.36 ± 0.06	136 ± 1
Linear fitting for runs on LiNaK carbonatite-olivine (450° to 700°C)						
A261	0.5 ± 0.1	0.6 ± 0.1	2	342	1.66 ± 0.02	35 ± 1
A253	2.3 ± 0.3	2.1 ± 0.2	1.3	320	0.92 ± 0.10	35 ± 2
A249	2.3 ± 0.3	2.3 ± 0.3	2	336	1.56 ± 0.07	36 ± 1
A251	2.3 ± 0.3	2.2 ± 0.4	5	318	1.95 ± 0.06	36 ± 1
A250	2.3 ± 0.3	2.1 ± 0.3	10	330	2.17 ± 0.03	32 ± 1
A245	6.5 ± 0.4	6.3 ± 0.4	2	297	1.45 ± 0.05	36 ± 1
A246	20 ± 3	18 ± 1	2	297	1.38 ± 0.05	37 ± 1

*Data of the single-crystal olivine from two duplicate runs at 1 GPa and Ni—NiO buffer (*19*), with similar olivine composition and the same assembly design as in this study.

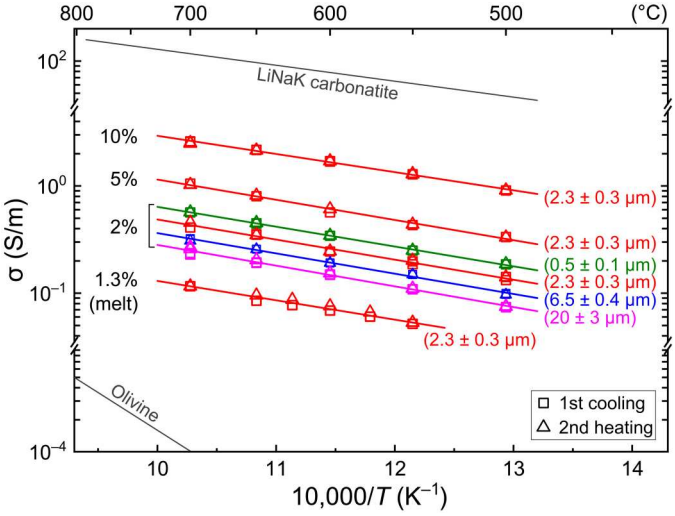

Fig. 1. Measured conductivity of LiNaK carbonatite-olivine. Mean olivine grain sizes and melt fractions are indicated. Colored lines are linear fittings to data in each run, and symbols of the same color are runs with the same olivine grain size. Data sources: LiNaK carbonatite, LiNaK carbonatite measured at room pressure (*4*); olivine, dry polycrystalline and single-crystal olivine (fig. S8). Uncertainty is usually smaller than or comparable to symbol sizes.

equilibrium in the samples, the melt geometry is affected by some mechanism(s), including the following: (i) the presence of electric charges, leading to charged layers, in grain boundaries (*27*–*29*); (ii) the occurrence of melt as isolated pockets and other forms (*21*, *30*), in addition to tubes or films that are widely used in grain boundary theoretical modeling; and/or (iii) the fact that the ideal packing of ordered and identical grains is never perfectly reached in natural and experimentally produced samples, causing the effect of grain size on melt topology (*25*).

Assuming that conductivity approaches certain asymptotic values at the large and small grain size limits, we propose the following relationship to model the effect of grain size (d) at the constant melt fraction (~2 vol %)

$$\sigma = \frac{\sigma_\infty - \sigma_0}{2}\tanh\left(\log\frac{d}{d_0}\right) + \frac{\sigma_\infty + \sigma_0}{2} \quad (2)$$

where σ_∞ and σ_0 are the conductivity at infinitely large and 0 grain size, respectively; tanh is the hyperbolic function; and d_0 is the critical grain size below which the grain size effect of melt becomes more important. σ_∞ corresponds to the "intrinsic" conductivity of the melt-olivine mixture, and σ_0 corresponds to the conductivity of the system with an infinitely small dimension of melt that differs from the bulk conductivity. The results demonstrate that σ_∞ and σ_0 are both temperature-dependent, and d_0 is less sensitive to temperature, with a mean value of ~2.27 μm (table S2). Experimental studies have shown the absence of apparent kinks/curvatures in the conductivity plot up to ~1400°C for lattice conduction in dry olivine (e.g., hoppings of electron holes between Fe^{2+} and Fe^{3+}), as demonstrated for polycrystalline (fig. S8) and single-crystal olivine (*15*, *16*, *19*), and ionic conduction in carbonatite melts, as documented for carbonatites with a variety of compositions (*4*, *6*). Hence, the data could be extrapolated to a higher temperature, although our analyses were performed up to 700°C. The modeled conductivity of the system versus temperature and grain size is plotted in Fig. 2. General and consistent temperature-related trends are observed. The change of conductivity over the same range of grain size is larger at higher temperature, and the reduction of conductivity with increasing olivine grain size at a given temperature, the grain size effect on melt-olivine conductivity, is more profound at a smaller value, e.g., below the mean d_0 (~2.27 μm).

At given conditions, different melts are characterized by different dihedral angles (and wetting abilities), e.g., ~10° to 40° for basalt-olivine and 10° to 30° for carbonatite-olivine (*20*, *24*, *31*), and conductivities, e.g., ~28 S/m for Ca- and Mg-rich mantle carbonatite (*5*) and 3 S/m for mantle basalt (*32*) at 1300°C that are less conductive than LiNaK carbonatite, which is not typical in the mantle, 550 S/m (*4*). In a melt-mineral mixture where the equilibrium melt distribution is acquired (e.g., a partially molten rock), however, the bulk conductivity under fixed conditions is controlled mainly by conductivity of the constitutive melt and mineral(s) as well as connectivity and topology of melt in the system. Grain size is of critical importance in determining the bulk conductivity, and its effect on melt-olivine conductivity is independent of the conductivity of melt itself (see Materials and Methods). We suggest that the general reduction of conductivity with increasing olivine grain size observed for the LiNaK carbonatite-olivine system is applicable to other melts (and even fluids). In many available studies, the conductivity of partially molten peridotites is estimated from basalt/carbonatite and olivine, by some mixing solutions including the Hashin-Shitrikman upper and lower bounds and the parallel and series models (*1*, *4*–*7*). To assess the effect of mineral grain size on the modeling, we calculate the bulk conductivity of the melt-olivine samples as a function of melt fraction and olivine grain size, with the conductivity data in this study and those of LiNaK carbonate in a previous report (*4*). The calculation is performed at 600°C using the measured data and Eq. 2, the parameters in table S2, and the mixing models. The results show that, for the Hashin-

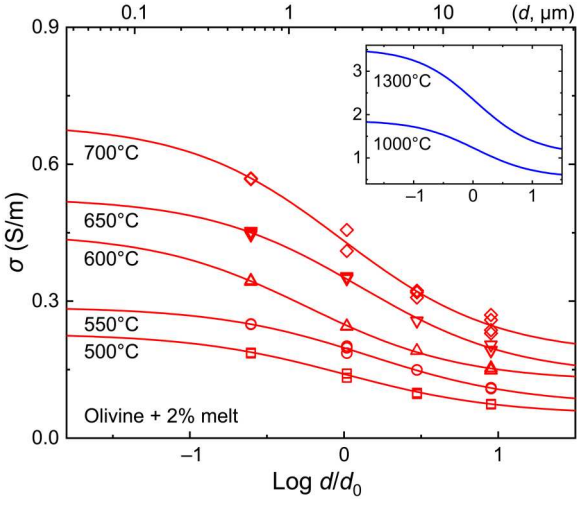

Fig. 2. Measured conductivity of LiNaK carbonatite-olivine versus grain size. Data are for samples with 2 vol % of LiNaK carbonatite (Fig. 1), and curves are by applying Eq. 2 to the data at each temperature. The inset is the fits by Eq. 2 to the conductivity data at 1000° and 1300°C extrapolated with Eq. 1 and parameters in Table 1, which are used to show the compatible temperature-related trends observed at low temperature.

Shitrikman upper bound and the parallel model that are widely adopted, the yielded conductivities are much greater, by a factor of ~5 to 26 that is larger at a smaller melt fraction, than the measured values, and those inferred by Eq. 2, of the samples with olivine grain sizes of ~0.5 to 20 μm (Fig. 3; similar grain size effect holds for other temperatures). The mixing models work for a melt-olivine mixture exclusively by assuming all melt in the form of tubes/films and complete wetting of grain boundaries by melt (0° dihedral angle). These assumptions are, however, hard to meet for basalt and carbonatite melts under shallow Earth conditions, because they occur only partly as tubes/films, with some as isolated pockets and other forms (*21*, *30*) that do not contribute to the bulk conductivity, and their dihedral angles with olivine (and other minerals) are usually >10°, not 0° (*20*, *24*, *31*). This causes the higher conductivity of the Hashin-Shitrikman upper bound and the parallel model.

Consequently, the studies on the bulk conductivity of a melt-olivine mixture without considering the grain size of olivine, e.g., by measuring the conductivity of mantle melt and olivine separately and estimating the bulk value or by determining the conductivity of the mixed melt-olivine directly using fine-grained olivine, greatly overestimate the conductivity, when the data are applied to the upper mantle where the mineral grain size is different. Volcano-hosted peridotite xenoliths, which sampled the upper mantle, have shown much larger grain sizes of olivine (and other main minerals). Typically, the grain size is 2 to 3 mm, but it can be >5 mm, in peridotites that are expected to dominate the upper mantle and is tens to hundreds of micrometers in strongly sheared peridotites that are limited to local regions (*33*, *34*). Hence, there is a large gap between the conductivity inferred from a melt and olivine or measured from a melt-olivine mixture and the actual value of partially molten peridotites in the mantle. The conductivity is overestimated by ~1 log unit if considering the typical grain sizes of mantle olivine

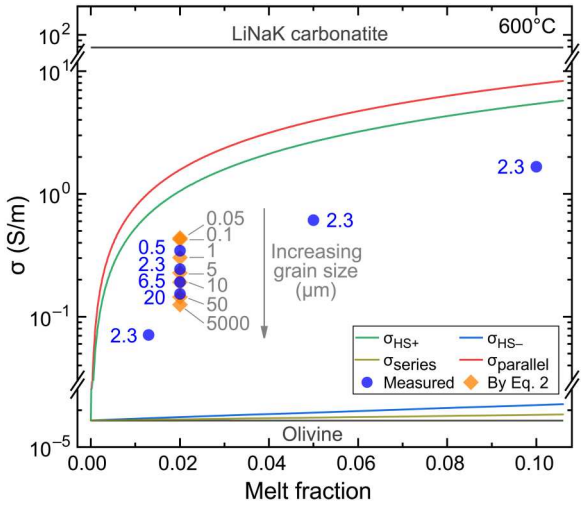

Fig. 3. Modeled conductivity of LiNaK carbonatite-olivine versus melt fraction and grain size at a fixed temperature. Modeling is conducted at 600°C with the conductivity of LiNaK carbonatite (*4*) and olivine (this study), using the Hashin-Shtrikman upper (σ_{HS+}) and lower (σ_{HS-}) bounds and the parallel ($\sigma_{parallel}$) and series (σ_{series}) models. The grain size effect on the melt-olivine conductivity is more remarkable at small grain sizes of olivine (see Results and Discussion and Fig. 2), and the uncertainty by extrapolating to mantle grain sizes is unlikely to be significant.

(Fig. 3), by taking into account the grain size effect on melt-olivine conductivity for the LiNaK carbonatite (as mentioned above). An immediate conclusion is that the required amount of melt for high conductivities in the shallow mantle, e.g., ~0.5 to 1 vol % of basalt or 0.05 to 0.5 vol % of carbonatite or carbonated basalt as proposed previously (*1*, *3*–*7*), is probably underestimated by ~1 order of magnitude. This estimate is meaningful when the enhanced conductivity of a mixed system at larger melt fractions (and otherwise identical conditions) is considered (fig. S9), although we are unable to directly calculate the conductivity of basalt-olivine and mantle carbonatite-olivine (at mantle grain sizes) because their σ_∞ and σ_0 are unknown. For melt that can be present in the shallow mantle, the fraction that is stable at a depth of <110 km is advocated to be <1 vol % and mostly <0.1 vol % away from mid-ocean ridges for basalt and <0.024 vol % for carbonatite (*9*–*11*). Hence, the effect of partial melt on many conductive regions in the asthenosphere is smaller than previous estimates.

In this case, the conductivity anomalies must be accounted for by other mechanism(s), probably except for some restricted zones right beneath, for example, mid-ocean ridges or hot spots where melt may be locally abundant. Conduction by subsolidus mantle materials is most likely. Various candidates have been proposed, including enriched water (structural OH) in olivine (*35*, *36*), oxidized state in the shallow mantle (*19*), grain boundary graphite films (*37*), iron- and water-rich pyroxenites (*38*), fluorine-rich phlogopite (*39*), sheared fine-grained olivine (*40*), and high-temperature–related ionic (Mg) conduction (*41*). Any successful (subsolidus) model must explain high and highly anisotropic conductivity and must also be consistent with geophysical and geochemical constraints on the lithosphere-asthenosphere structures, including the rheological and compositional stratification (*42*–*46*), the depth variation in the redox state (*47*), and the seismic anisotropy (*48*). Developing such a model will help us to better understand the structure and dynamics of the lithosphere-asthenosphere system. Last, the grain size effect should be taken into account for inferring the bulk conductivity of any other melt- or fluid-bearing systems in the crust and mantle.

MATERIALS AND METHODS

Starting materials and sample characterization

The starting materials were gem-quality olivine single crystals from Northeast China and nanosized reagent carbonatites—Li_2CO_3, Na_2CO_3, and K_2CO_3. Olivine, originally dry, was ground and sieved into different grain size fractions with an agate mortar and pestle under alcohol and a ball mill. Geometry of olivine grains is key for topology of grain boundary melt. We initially tried to anneal olivine and LiNaK carbonatite at 1 GPa and 700°C for a long duration (>240 hours; in a piston cylinder press), but the yielded olivine always contained some water (by incorporation of adsorbed moisture). The water content is hard to control, and it is difficult to produce samples with the same water content. This affects conductivity analysis, and we used another method. Olivine powder was first annealed with distilled water in Ni capsules at 0.6 GPa and 1000° to 1100°C (5 to 20 hours; in piston cylinder press) for grain growth and then dehydrated in a CO—CO_2 mixing furnace at 1000°C (~24 hours, 1 bar) for obtaining dry olivine, with redox state set close to the Ni—NiO buffer. The low-pressure annealing under water-rich conditions did not strongly sinter

mineral grains. The annealed olivine was slightly crushed, sieved, and mixed with the LiNaK carbonatite for conductivity runs. Water in olivine was examined using a Bruker Vertex 70V FTIR spectrometer and a Hyperion 2000 microscope. Olivine composition was measured with a JXA8230 electron microprobe (EMP), and olivine grain size was measured using a Hitachi S3400N scanning electron microscope (SEM).

Conductivity runs

Assembly design (fig. S1) follows that in other studies (*17*–*19*, *38*, *39*, *49*–*52*). A U-shaped Ni capsule and a soft highly resistive hexagonal boron-nitride (BN) capsule bearing sample, Pt electrodes, Ni-NiO buffer and a type-S thermocouple are used. The double-capsule design maintains sample geometry, and yields a closed chamber. This minimizes sample distortion and avoids graphite diffusion into pressure medium/sample inside capsules. Redox state in the capsule is well buffered, as assessed for Fe^{3+} in olivine and pyroxenes (*17*, *38*, *49*, *53*), and sample Fe loss to electrodes is insignificant (*17*, *19*). To avoid volatile release that affects impedance analyses, Al_2O_3 parts were pre-heated at 1000°C to remove adsorbed water, and no cement or glue was used to immobilize assembly parts. Completed assembly was heated at 136°C for ~24 hours. After loading into press and reaching the target pressure, sample was heated again at 200°C. Temperature ramped at 10–30°C/min, and was ≤700°C in the carbonatite-bearing samples to avoid decarbonation (*13*). Over run conditions, sample resistance, >700 ohm for 1.3 and 2 vol % of melt and >130 ohm for 10 vol % of melt, is much larger than wire resistance (<1 ohm). Thus, impedance can be measured by the two-wire method, without the necessity to use more a demanding four-wire configuration. Typical impedance spectra are given in fig. S2.

Recovered samples

After conductivity runs, recovered samples were carefully examined. The Ni—NiO pair was still present, and no water was detected in olivine. Sample distortions were weak, as documented in similar works (*17*–*19*, *38*, *39*, *49*–*52*). Equilibrium of olivine geometry is reached (fig. S3). LiNaK carbonatite is unquenchable, amorphous, and highly soluble in water and was lost during polishing, making them (except for some spots) hard to observe on exposed surfaces. This has also been reported for Ca- and Mg-rich carbonatites in conductivity runs (*5*). The textural equilibrium is also supported by the systematic grain size effect on the conductivity of the melt-olivine samples over the studied grain sizes. One thing that should be mentioned is that, in an ideal system (identical grains and ordered packing), the textural equilibrium of all grains might be fully reached. In natural and experimentally yielded samples, however, the equilibrium is hard to establish for all grains and is usually reached for most of them, owing to non-identical grains, non-ordered packing, voids, and/or other reasons as shown previously (*5*, *7*, *54*–*56*). Open voids are observed in our melt-absent samples, similar to previous studies for polycrystalline olivine annealed at 0.3 to 9.6 GPa and 1000° to 1600°C (*57*, *58*). Sample dihedral angle (fig. S4) is measured from the observed apparent dihedral angle, following established protocols (*54*–*56*). Grain sizes of olivine (fig. S5) were determined by analyzing grain area and estimating the mean value of the equivalent circular grain diameters (using Nano Measurer software).

Self-similar melt geometry in ideal melt-bearing system

In a melt-mineral mixture, e.g., a partially molten rock, melt exists with a certain geometry, e.g., tubes, films, or isolated pockets. Concerning connected tubes/films at a given dihedral angle that controls the melt geometry, the melt fraction in ideal cases (e.g., identical grains and ordered packing) is proportional to $(\delta/d)^n$, where δ is the dimension of tubes/films (tube diameter/film thickness) at a given grain size and n is 2 for tubes and 1 for films. Thus, δ/d is a constant at a fixed melt fraction [the self-similar melt geometry as often referred to (*31*)]. Then, the bulk conductivity of a melt-olivine mixture, if controlled by melt geometry only, would be proportional to $(\delta/d)^n$ that is grain size independent.

Data modeling

Mixing solutions for modeling melt-olivine conductivity include the following: Series model $\sigma_{series}^{-1} = x_{melt} / \sigma_{melt} + x_{oli} / \sigma_{oli}$; Parallel model $\sigma_{parallel} = x_{melt} \cdot \sigma_{melt} + x_{oli} \cdot \sigma_{oli}$; Hashin-Shtrikman upper bound $\sigma_{HS+} = \sigma_{melt} + x_{oli} \cdot [(\sigma_{oli} - \sigma_{melt})^{-1} + x_{melt}/(3 \cdot \sigma_{melt})]^{-1}$; Hashin-Shtrikman lower bound $\sigma_{HS-} = \sigma_{oli} + x_{melt} \cdot [(\sigma_{melt} - \sigma_{oli})^{-1} + x_{oli}/(3 \cdot \sigma_{oli})]^{-1}$ where $\sigma_{melt,oli}$ and $x_{melt,oli}$ are the conductivity and volume fraction of the melt and olivine, respectively. The Archie's law (*59*), $\sigma = C \cdot \sigma_{melt} \cdot x_{melt}^n$, where C and n are material-related factors, is often used to model bulk conductivity of a melt-solid mixture; however, it requires already known C and n, and the modeled data are usually close to σ_{HS+}.

Grain size–sensitive transport of melt in Earth materials is often described by a power-law relation (*25*). The reduced conductivity with olivine grain size at a fixed melt fraction is modeled by $\sigma = A' \cdot \frac{1}{d^m} \cdot \exp\left(-\frac{\Delta H'}{RT}\right)$, where A' is a constant, m is an exponential factor, and $\Delta H'$ is the activation enthalpy. This is more straightforward in linking grain size to bulk conductivity, although it produces biased values at infinitely large/small grain sizes. Fitting the measured data of samples with 2 vol % of melt to this relation, by a multilinear regression, yields log(A', S/m) of 0.30 ± 0.03, m of 0.24 ± 0.01, and $\Delta H'$ of 36 ± 1 kJ/mol (r^2 = 0.99). The conductivity, if normalized to a reference value (σ_{ref}) at a presumed reference grain size (d_{ref}) and the same T, is given by $\frac{\sigma}{\sigma_{ref}} = \left(\frac{d_{ref}}{d}\right)^{0.24}$. Then, the grain size effect on the melt-olivine conductivity, the relative variation of conductivity (σ_1 and σ_2) versus grain size (d_1 and d_2, assuming $d_1 < d_2$ that leads to $\sigma_1 > \sigma_2$) at a fixed T, is $\frac{\sigma_1 - \sigma_2}{\sigma_1} = 1 - \left(\frac{d_1}{d_2}\right)^{0.24}$ or $\frac{\sigma_2}{\sigma_1} = \left(\frac{d_1}{d_2}\right)^{0.24}$, which is independent of melt conductivity. This applies to other melts, although it is unclear if the same m value holds [note that similar analyses cannot be accurately done for mantle basalt and carbonatite at >1200°C (see Introduction)].

Supplementary Materials

This PDF file includes:

Figs. S1 to S9
Tables S1 and S2
References

REFERENCES AND NOTES

1. T. J. Shankland, H. S. Waff, Partial melting and electrical conductivity anomalies in the upper mantle. *J. Geophys. Res.* **82**, 5409–5417 (1977).

2. R. L. Evans, G. Hirth, K. Baba, D. Forsyth, A. Chave, R. Mackie, Geophysical evidence from the MELT area for compositional controls on oceanic plates. *Nature* **437**, 249–252 (2005).
3. S. Naif, K. Key, S. Constable, R. L. Evans, Melt-rich channel observed at the lithosphere-asthenosphere boundary. *Nature* **495**, 356–359 (2013).
4. F. Gaillard, M. Malki, G. Iacono-Marziano, M. Pichavant, B. Scaillet, Carbonatite melts and electrical conductivity in the asthenosphere. *Science* **322**, 1363–1365 (2008).
5. T. Yoshino, M. Laumonier, E. McIsaac, T. Katsura, Electrical conductivity of basaltic and carbonatite melt-bearing peridotites at high pressures: Implications for melt distribution and melt fraction in the upper mantle. *Earth Planet. Sci. Lett.* **295**, 593–602 (2010).
6. D. Sifré, L. Hashim, F. Gaillard, Effects of temperature, pressure and chemical compositions on the electrical conductivity of carbonated melts and its relationship with viscosity. *Chem. Geol.* **418**, 189–197 (2015).
7. M. Laumonier, R. Farla, D. J. Frost, T. Katsura, K. Marquardt, A.-S. Bouvier, L. P. Baumgartner, Experimental determination of melt interconnectivity and electrical conductivity in the upper mantle. *Earth Planet. Sci. Lett.* **463**, 286–297 (2017).
8. D. Blatter, S. Naif, K. Key, A. Ray, A plume origin for hydrous melt at the lithosphere–asthenosphere boundary. *Nature* **604**, 491–494 (2022).
9. D. McKenzie, The extraction of magma from the crust and mantle. *Earth Planet. Sci. Lett.* **74**, 81–91 (1985).
10. T. Plank, C. H. Langmuir, Effects of the melting regime on the composition of the oceanic crust. *J. Geophys. Res.* **97**, 19749–19770 (1992).
11. M. Hirschmann, Partial melt in the oceanic low velocity zone. *Phys. Earth Planet. In.* **179**, 60–71 (2010).
12. S.-i. Karato, Does partial melting explain geophysical anomalies? *Phys. Earth Planet. In.* **228**, 300–306 (2014).
13. R. I. Olivares, C. Chen, S. Wright, The thermal stability of molten lithium–sodium–potassium carbonate and the influence of additives on the melting point. *J. Sol. Energy Eng.* **134**, 041002 (2012).
14. J. S. Huebner, R. G. Dillenburg, Impedance spectra of hot, dry silicate minerals and rock: Qualitative interpretation of spectra. *Am. Mineral.* **80**, 46–64 (1995).
15. Y. Xu, T. J. Shankland, A. G. Duba, Pressure effect on electrical conductivity of mantle olivine. *Phys. Earth Planet. In.* **118**, 149–161 (2000).
16. B. T. Poe, C. Romano, F. Nestola, J. R. Smyth, Electrical conductivity anisotropy of dry and hydrous olivine at 8 GPa. *Phys. Earth Planet. In.* **181**, 103–111 (2010).
17. X. Yang, H. Keppler, C. McCammon, H. Ni, Q.-K. Xia, Q. Fan, Effect of water on the electrical conductivity of lower crustal clinopyroxene. *J. Geophys. Res.* **116**, B04208 (2011).
18. X. Yang, F. Heidelbach, Grain size effect on the electrical conductivity of clinopyroxene. *Contrib. Mineral. Petrol.* **163**, 939–947 (2012).
19. H. Liu, Q. Zhu, X. Xu, H. Fei, X. Yang, High electrical conductivity of olivine at oxidizing conditions of the shallow mantle and geophysical implications. *J. Geophys. Res.* **126**, e2021JB022739 (2021).
20. W. G. Minarik, E. B. Watson, Interconnectivity of carbonate melt at low melt fraction. *Earth Planet. Sci. Lett.* **133**, 423–437 (1995).
21. T. Hammouda, D. Laporte, Ultrafast mantle impregnation by carbonatite melts. *Geology* **28**, 283–285 (2000).
22. A. Shatskiy, K. D. Litasov, Y. M. Borzdov, T. Katsura, D. Yamazaki, E. Ohtani, Silicate diffusion in alkali-carbonatite and hydrous melts at 16.5 and 24 GPa: Implication for the melt transport by dissolution–precipitation in the transition zone and uppermost lower mantle. *Phys. Earth Planet. In.* **225**, 1–11 (2013).
23. M. Toriumi, A mechanism of shape-transformation of quartz inclusions in albite of regional metamorphic rocks. *Lithos* **12**, 325–333 (1979).
24. R. F. Cooper, D. L. Kohlstedt, Rheology and structure of olivine-basalt partial melts. *J. Geophys. Res.* **91**, 9315–9323 (1986).
25. D. A. Wark, E. B. Watson, Effect of grain size on the distribution and transport of deep-seated fluids and melts. *Geophys. Res. Lett.* **27**, 2029–2032 (2000).
26. J. J. Roberts, J. A. Tyburczy, Frequency dependent electrical properties of polycrystalline olivine compacts. *J. Geophys. Res.* **96**, 16205–16222 (1991).
27. W. D. Kingery, Plausible concepts necessary and sufficient for interpretation of ceramic grain-boundary phenomena: I, grain-boundary characteristics, structure, and electrostatic potential. *J. Am. Ceram. Soc.* **57**, 1–8 (1974).
28. W. D. Kingery, Plausible concepts necessary and sufficient for interpretation of ceramic grain-boundary phenomena: II, solute segregation, grain-boundary diffusion, and general discussion. *J. Am. Ceram. Soc.* **57**, 74–83 (1974).
29. S. F. Gurmani, S. Jahn, H. Brasse, F. R. Schilling, Atomic scale view on partially molten rocks: Molecular dynamics simulations of melt-wetted olivine grain boundaries. *J. Geophys. Res.* **116**, B12209 (2011).
30. K. J. Miller, W.-l. Zhu, L. G. Montési, G. A. Gaetani, V. Le Roux, X. Xiao, Experimental evidence for melt partitioning between olivine and orthopyroxene in partially molten harzburgite. *J. Geophys. Res. Solid Earth* **121**, 5776–5793 (2016).
31. B. K. Holtzman, Questions on the existence, persistence, and mechanical effects of a very small melt fraction in the asthenosphere. *Geochem. Geophys. Geosyst.* **17**, 470–484 (2016).
32. J. A. Tyburczy, H. S. Waff, Electrical conductivity of molten basalt and andesite to 25 kilobars pressure: Geophysical significance and implications for charge transport and melt structure. *J. Geophys. Res.* **88**, 2413–2430 (1983).
33. J. C. C. Mercier, A. Nicolas, Textures and fabrics of upper-mantle peridotites as illustrated by xenoliths from basalts. *J. Petrol.* **16**, 454–487 (1975).
34. F. A. Tabor, B. E. Tabor, H. Downes, Quantitative characterization of textures in mantle spinel peridotite xenoliths. *Geol. Soc. Lond. Spec. Publ.* **337**, 195–211 (2010).
35. S. Karato, The role of hydrogen in the electrical conductivity of the upper mantle. *Nature* **347**, 272–273 (1990).
36. L. Dai, S. Karato, High and highly anisotropic electrical conductivity of the asthenosphere due to hydrogen diffusion in olivine. *Earth Planet. Sci. Lett.* **408**, 79–86 (2014).
37. A. G. Duba, T. J. Shankland, Free carbon and electrical conductivity in the Earth's mantle. *Geophys. Res. Lett.* **9**, 1271–1274 (1982).
38. X. Yang, C. McCammon, Fe^{3+}-rich augite and high electrical conductivity in the deep lithosphere. *Geology* **40**, 131–134 (2012).
39. Y. Li, X. Yang, J. Yu, Y. Cai, Unusually high electrical conductivity of phlogopite: The possible role of fluorine and geophysical implications. *Contrib. Mineral. Petrol.* **171**, 37 (2016).
40. A. Pommier, D. L. Kohlstedt, L. N. Hansen, S. Mackwell, M. Tasaka, F. Heidelbach, K. Leinenweber, Transport properties of olivine grain boundaries from electrical conductivity experiments. *Contrib. Mineral. Petrol.* **173**, 41 (2018).
41. H. Fei, D. Druzhbin, T. Katsura, The effect of water on ionic conductivity in olivine. *J. Geophys. Res. Solid Earth* **125**, e2019JB019313 (2020).
42. S. Karato, Grain-size distribution and rheology of the upper mantle. *Tectonophysics* **104**, 155–176 (1984).
43. G. Hirth, D. L. Kohlstedt, Water in the oceanic upper mantle: Implications for rheology, melt extraction and the evolution of the lithosphere. *Earth Planet. Sci. Lett.* **144**, 93–108 (1996).
44. S. Karato, H. Jung, Water, partial melting and the origin of the seismic low velocity and high attenuation zone in the upper mantle. *Earth Planet. Sci. Lett.* **157**, 193–207 (1998).
45. S. Karato, On the origin of the asthenosphere. *Earth Planet. Sci. Lett.* **321**–**322**, 95–103 (2012).
46. S. Masuti, S. Barbot, S. Karato, L. Feng, P. Banerjee, Upper-mantle water stratification inferred from observations of the 2012 Indian Ocean earthquake. *Nature* **538**, 373–377 (2016).
47. D. J. Frost, C. A. McCammon, The redox state of Earth's mantle. *Annu. Rev. Earth Planet. Sci.* **36**, 389–420 (2008).
48. S. Karato, H. Jung, I. Katayama, P. Skemer, Geodynamic significance of seismic anisotropy of the upper mantle: New insights from laboratory studies. *Annu. Rev. Earth Planet. Sci.* **36**, 59–95 (2008).
49. X. Yang, H. Keppler, C. McCammon, H. Ni, Electrical conductivity of orthopyroxene and plagioclase in the lower crust. *Contrib. Mineral. Petrol.* **163**, 33–48 (2012).
50. Y. Li, H. Jiang, X. Yang, Fluorine follows water: Effect on electrical conductivity of silicate minerals by experimental constraints from phlogopite. *Geochim. Cosmochim. Acta* **217**, 16–27 (2017).
51. H. Liu, Q. Zhu, X. Yang, Electrical conductivity of OH-bearing omphacite and garnet in eclogite: The quantitative dependence on water content. *Contrib. Mineral. Petrol.* **174**, 57 (2019).
52. H. Liu, K. Zhang, J. Ingrin, X. Yang, Electrical conductivity of omphacite and garnet indicates limited deep water recycling by crust subduction. *Earth Planet. Sci. Lett.* **559**, 116784 (2021).
53. X. Yang, Orientation-related electrical conductivity of hydrous olivine, clinopyroxene and plagioclase and implications for the structure of the lower continental crust and uppermost mantle. *Earth Planet. Sci. Lett.* **317**–**318**, 241–250 (2012).
54. R. H. Hunter, D. McKenzie, The equilibrium geometry of carbonate melts in rocks of mantle composition. *Earth Planet. Sci. Lett.* **92**, 347–356 (1989).
55. J. Maumus, D. Laporte, P. Schiano, Dihedral angle measurements and infiltration property of SiO_2-rich melts in mantle peridotite assemblages. *Contrib. Mineral. Petrol.* **148**, 1–12 (2004).
56. E. B. Watson, J. M. Brenan, D. R. Baker, Distribution of fluids in the continental mantle, in *Continental Mantle*, M. A. Menzies, Ed. (Oxford Univ. Press, 1990), pp. 111–125.
57. S. Demouchy, A. Tommasi, F. Barou, D. Mainprice, P. Cordier, Deformation of olivine in torsion under hydrous conditions. *Phys. Earth Planet. In.* **202**–**203**, 56–70 (2012).
58. T. Kawazoe, S.-i. Karato, K. Otsuka, Z. Jing, M. Mookherjee, Shear deformation of dry polycrystalline olivine under deep upper mantle conditions using a rotational Drickamer apparatus (RDA). *Phys. Earth Planet. In.* **174**, 128–137 (2009).
59. G. E. Archie, The electrical resistivity log as an aid in determining some reservoir characteristics. *Trans. AIME* **146**, 54–62 (1942).

60. R. F. Wendlandt, J. S. Huebner, W. J. Harrison, The redox potential of boron nitride and implications for its use as a crucible material in experimental petrology. *Am. Mineral.* **67**, 170–174 (1982).

Acknowledgments: We thank K. Zhang and Q. Zhu for assistance in piston cylinder experiments and data modeling, G. Hirth and three anonymous referees for comments, and G. Gaetani for editorial handling. X.Y. thanks D. Kohlstedt for open discussions on the early preliminary results of the work. **Funding:** This study was supported by the National Science Foundation of China (42230301 and 41725008), Research Funds for the Frontiers Science Center for Critical Earth Material Cycling, and Fundamental Research Funds for the Central Universities to X.Y. **Author contributions:** X.Y. conceived the ideas, organized the project, explained the data, and wrote the manuscript. H.L. conducted the sample preparation; conductivity experiments; and FTIR, SEM, and EMP analyses. S.-i.K. proposed to fit the data with Eq. 2 and modeled the ideal self-similar geometry of melt in Materials and Methods. All authors contributed to the experiments and the final manuscript. **Competing interests:** The authors declare that they have no competing interests. **Data and materials availability:** All data needed to evaluate the conclusions in the paper are present in the paper and/or the Supplementary Materials.

Submitted 30 April 2022
Accepted 1 March 2023
Published 31 March 2023
10.1126/sciadv.abq7884